

A threshold photoelectron-photoion coincidence spectrometer with double velocity imaging using synchrotron radiation

Xiaofeng Tang,¹ Xiaoguo Zhou,^{1,a)} Mingli Niu,¹ Shilin Liu,^{1,a)} Jinda Sun,² Xiaobin Shan,² Fuyi Liu,² and Liusi Sheng²

¹Hefei National Laboratory for Physical Sciences at the Microscale, Department of Chemical Physics, University of Science and Technology of China, Hefei, Anhui 230026, People's Republic of China

²National Synchrotron Radiation Laboratory, University of Science and Technology of China, Hefei, Anhui 230029, People's Republic of China

(Received 9 August 2009; accepted 28 September 2009; published online 2 November 2009)

A novel threshold photoelectron-photoion coincidence (TPEPICO) imaging spectrometer at the U14-A beamline of the Hefei National Synchrotron Radiation Laboratory is presented. A set of open electron and ion lenses are utilized to map velocity imaging of photoelectrons and photoions simultaneously, in which a repelling electric field using an extra lens is applied to magnify images of photoelectrons instead of traditional accelerating electric field in order to suppress the contribution of energetic electrons in the threshold photoelectron spectroscopy (TPES) and the mass-selected TPEPICO spectroscopy. The typical energy resolution of TPES is measured to be 9 meV (full width at half maximum), as shown on the $^2P_{1/2}$ ionization of argon. The measured mass resolving power for the present TPEPICO imaging spectrometer is above 900 of $M/\Delta M$. Subsequently as a benchmark, oxygen molecule is photoionized by monochromatic synchrotron radiation at 20.298 eV and dissociates to an oxygen atomic ion and a neutral oxygen atom, and the translation energy distribution of oxygen atomic ion is measured by the time-sliced imaging based on mass-selected TPEPICO experiment. The kinetic energy resolution of the present ion velocity imaging is better than 3% of $\Delta E/E$. © 2009 American Institute of Physics.

[doi:10.1063/1.3250872]

I. INTRODUCTION

Photoionization dynamics of gaseous molecules have been investigated for more than half a century as a basic and common photon-matter process in nature, and its understanding is of fundamental importance to physics, chemistry, and biology. In order to ionize a molecule using a single photon in laboratory, short wavelength light sources such as discharge lamps, vacuum ultraviolet (VUV) laser, and synchrotron radiation (SR) are necessary, as most molecules have the ionization energies (IE) of about 10 eV in the VUV photon energy range. Among all the VUV light sources, SR has special advantages like wide and tunable wavelength range, and hence it is believed to be a favorable light source for investigation of photoionization dynamics of molecules. Therefore, a lot of experimental investigations of molecular photoionization have been performed using SR.¹⁻⁸

Photoelectron-photoion coincidence (PEPICO) spectroscopy is a powerful approach to prepare and analyze the state-selected ions, and has been applied for a long history.⁹⁻¹² The principle of PEPICO is that when a molecule is photoionized, the internal energy of ion is related with the kinetic energy of photoelectron from the energy conservation.¹³ Based on differences of light sources and kinetic energies of the detected electrons, two types of PEPICO spectroscopy have been developed in laboratory: (a) a fixed energy light

source is used and the ions are measured in coincidence with energy-selected electrons by a dispersive energy analyzer;^{9,10} (b) a variable energy light source is employed and only initially zero energy photoelectrons, so-called threshold photoelectrons, are detected in coincidence with the ions, which is often defined as threshold PEPICO (TPEPICO).¹²⁻¹⁷ As TPEPICO technique has the virtues of much higher collection efficiency and higher energy resolution for threshold electrons, it is believed to be a more applicable tool to study photoionization of molecules. Furthermore, when energy of parent ion is above the dissociation limit and a rapid dissociative photoionization (DPI) process happens, a lot of information about molecular photoionization and DPI dynamics, like IE, dissociation limit, appearance energy, heat of formation, and kinetic energy released (KER) from the state-selected parent ions, can be obtained through the TPEPICO experiments.^{1-4,13-19}

However, the major disadvantage in TPEPICO measurement is the contamination of the collected threshold electron by energetic electrons, which are difficult to fully distinguish from the true threshold electrons. To select the threshold electrons from all, the simplest way is to use a steradiancy analyzer which consists of a drift tube with a small aperture.^{20,21} However, it is impossible to fully eliminate the contamination by using this approach, since those energetic electrons with initial velocity vectors along the direction of detector will be collected regardless of their energy.¹³ Another two approaches have been performed to select thresh-

^{a)} Authors to whom correspondence should be addressed. Electronic addresses: xzhou@ustc.edu.cn and slliu@ustc.edu.cn.

old electrons by using an achromatic extraction lens or a penetrating field followed by a dispersive analyzer.^{22–24} Since the SR photoionization region is much larger than that the analyzer generally requires, the voltage drop in the region causes a larger energy range of the produced electrons than the expected resolution of several meV. Moreover, it has another serious disadvantage of a low collection efficiency of threshold electrons, and thus the dispersive analyzer has been seldom used in SR-based TPEPICO experiments. When a pulsed light source like SR operated in single bunch mode is used, energetic electrons can be effectively suppressed with the selection of true threshold electrons based on electron time of flight (TOF).^{25–27} Weitzel and Guthe combined pulsed field ionization (PFI) and single bunch SR to detect threshold electrons, and got a high resolution PFI photoelectron spectrum.²⁸ However, single bunch operation of modern SR is not a practical application of the beam current and thus tends to be discouraged. An ingenious PFI-PEPICO technique using the multibunch SR has been developed by Ng and co-workers^{17,29,30} using PFI at the Advanced Light Source. Molecules which have been excited by quasicontinuous SR to the high- n Rydberg states are field-ionized by the application of a small pulse field (0.5 V/cm). A dark gap of the SR, about 100 ns, permits sufficient time to pulsed push electrons out of ionization region, and thus threshold electrons can be efficiently discriminated from energetic electrons by different flight times. Although this approach provides a very high electron energy resolution of 0.1 meV, the PFI-PEPICO has inherent disadvantages of low signal level and structured background in mass spectra due to the pulsed extraction electric field.

In previous TPEPICO experiments, a low electric field to collect electrons is necessary to reduce the contamination of energetic electrons and achieve high electron energy resolution, and thus a problem happens to impede achieving good mass resolution of ions, as good mass resolution requires high electric field. Therefore, an important factor to restrict previous TPEPICO studies is the difficult simultaneous optimization of the electron energy resolution and the ion TOF mass resolution when using a same extraction electric field. A new TPEPICO experimental method is welcome, if it can simultaneously increase the signal level of threshold electrons, suppress the energetic electrons and provide a satisfied mass resolution of ions.

Baer and co-workers^{18,31,32} have reported a significant improvement in collection efficiency and energy resolution of threshold electrons by applying velocity map imaging (VMI) technique in TPEPICO experiments. In VMI, all charged particles with the same momentum will be focused onto almost same spot on the detector, even if they are generated at different spatial positions usually covering several millimeters.^{33–35} The collection solid angle of charged particles can be increased to almost 4π sr with such designed velocity imaging optics, and the measured kinetic energy range of charged particles can be extended greatly. However, the energetic electrons with initial velocity vectors along the direction of detector do not change flying trajectories in VMI and will be collected mistakenly as threshold electrons. In order to get a high energy resolution for threshold electron,

both the center (threshold electrons and those energetic electrons with initial velocity vectors along the direction of detector) and off-axis (energetic electrons with perpendicular velocity components) electrons through VMI have been detected simultaneously in the experiments of Baer *et al.*, and then the true threshold photoelectron signals can be obtained by subtracting the off-axis signals from the center ones.^{18,32} More recently, Garcia *et al.*³⁶ and Bodi *et al.*³⁷ have respectively applied the VMI of electrons to their SR-based TPEPICO experiments. Using a similar subtraction way, Garcia *et al.*³⁶ have acquired the superhigh energy resolution of 0.8 meV in TPE spectroscopy (TPES). Bodi *et al.*³⁷ have improved the recording rate of TPES to over 100 kHz with a triggerless multiple-start/multiple-stop measurement mode. Subsequently, they have performed the DPI investigations of several molecules by combining with a linear TOF mass spectrometer to detect ions.^{36,37}

Among previous TPEPICO experiments, a linear or reflectron TOF mass spectrometer has been generally employed to detect ions. When a DPI process exists, the KER distribution (KERD) of fragment ions can be obtained from the simulation of TOF profile,^{4,19,38,39} but the results usually do not have sufficient energy resolution and angular distribution information. In contrast to the TOF technique, VMI of ions can simultaneously provide a better momentum resolution and information of angular distribution. Thus, we have applied the VMI to both photoelectrons and photoions in present TPEPICO spectrometer. Briefly, a moderate extraction electric field of TOF is used to facilitate the high transmission of both electrons and ions, in which a repelling electric field is utilized to magnify images of electrons in order to suppress the contamination of energetic electrons. In addition, a delicate VMI design is performed to measure the spatial and angular distribution of fragment ions. Therefore, this novel SR-based TPEPICO spectrometer with double velocity imaging is especially powerful to study DPI dynamics of molecules, besides that, TPES and TPEPICO spectra of molecules can be performed.

II. EXPERIMENTAL DESIGN

A. Light source

SR from an undulator-based U14-A beamline of 800 MeV electron storage ring at the National Synchrotron Radiation Laboratory, Hefei, China, is dispersed with a 6 m length monochromator, which is equipped with three gratings (370, 740, and 1250 grooves mm^{-1} , Horiba Jobin Yvon). Three gratings cover the photon energy from 7.5 to 22.5 eV for 370 grooves mm^{-1} , 15 to 45 eV for 740 grooves mm^{-1} , and 36 to 124 eV for 1250 grooves mm^{-1} , respectively. In the following experiments, only 370 grooves mm^{-1} grating is used and its energy resolving power ($E/\Delta E$) is above 2000 when the widths of the entrance and exit slits are adjusted to 80 μm . For instance, the energy resolution of photons at 15.9 eV is measured to be 6 meV [full width at half maximum (FWHM)],⁷ and the average photon flux is about 2.0×10^{12} photons s^{-1} . The absolute wavelength of monochromator was precisely calibrated with the known IEs of inert gases.

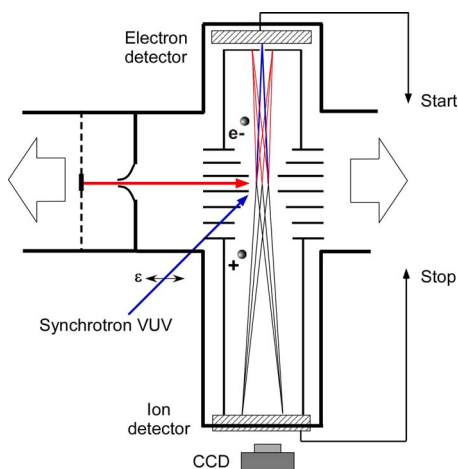


FIG. 1. (Color online) Schematic diagram of TPEPICO imaging spectrometer. The apparatus consists of two chambers, one is a supersonic MB chamber and the other is the detection chamber with the TPEPICO imaging spectrometer. The polarization of SR noted as ϵ is along the horizontal direction.

A gas filter filled with neon is mounted in front of our apparatus to eliminate higher order harmonic radiation of undulator. A silicon photodiode (SXUV-100, International Radiation Detectors Inc.) is used to monitor the photon flux for normalizing electron and ion signals.

B. Apparatus and molecular beam

A typical dual TOF mass spectrometer is the basic structure of our apparatus. In Fig. 1, we show a geometric schematic diagram of the whole experimental apparatus. The apparatus consists of two chambers, a source chamber and a detection chamber with the TPEPICO imaging mass spectrometer. Two chambers are separated by a 0.5 mm diameter skimmer (Beam Dynamics). To avoid contamination from the vacuum system, oil-free pumps are used in the whole apparatus. The source chamber has a 1800 l/s turbo molecular pump (KYKY, FF-250/1800), and the detection chamber is pumped by a 1600 l/s turbo molecular pump (Leybold, T1600). All turbo pumps are backed by a 253 $\text{m}^3 \text{h}^{-1}$ roots pump (Leybold, WA251) and a dry pump. The whole chamber, TOF tubes and electrodes are made of nonmagnetic stainless. All electrodes and TOF tubes in the spectrometer are magnetic shielded by a 1 mm thick μ -metal tube, to reduce the effect from the stray magnetic fields around.

A continuous supersonic molecular beam (MB) is generated through a homemade 30 μm diameter aperture, and the skimmer is positioned at 25 mm downstream from the nozzle. The typical backing pressure behind the nozzle is 1.2×10^5 Pa. The pressures of the two chambers are less than 1×10^{-5} Pa with the MB off, while they will be respectively increased to 2×10^{-3} and 4×10^{-5} Pa with the MB on. The MB is perpendicularly crossed by SR at about 100 mm downstream from the nozzle. As a result, the width of MB crossing with SR is estimated to be 3 mm along the direction of light propagation. As the size of the incoming SR is about $1 \times 4 \text{ mm}^2$ in photoionization region due to the restriction of an entrance slit, all charged particles are expected to generate within a volume of $1 \times 3 \times 4 \text{ mm}^3$.

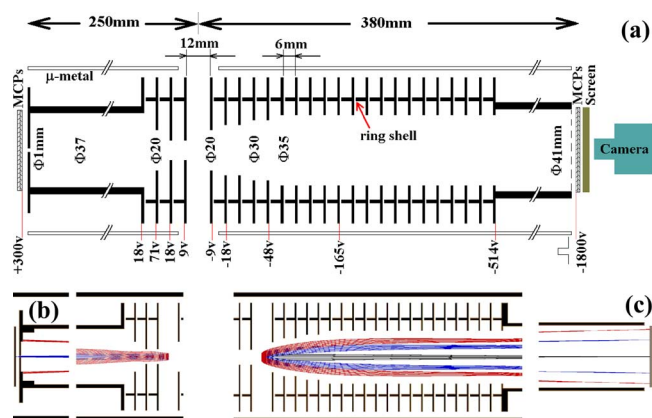


FIG. 2. (Color online) (a) Geometric diagram of the velocity focusing optics and dual TOF tubes in present TPEPICO imaging spectrometer; (b) simulated trajectories of the threshold (in blue) and 50 meV (in red) energetic electrons; (c) simulated trajectories of ions with zero (in black), 0.3 eV (in blue), and 0.8 eV (in red) kinetic energy. In all simulations above, the extraction field is 15 V cm^{-1} .

C. VMI for electrons and ions

Molecules are photoionized in the right crossing region of MB and SR, and the produced electrons and ions are pushed apart by a dc extraction electric field. A 1 mm diameter aperture is located at the end of electron drift tube to pass threshold electrons. In Fig. 2(a), a geometric diagram of the velocity focusing optics is shown. The trajectories of electrons and ions have been simulated with the SIMION 3D VER.7.0 program (Scientific Instrument Services, Inc.), and the potentials of all electrodes have been obtained to generate a satisfied ion optics and are presented in Fig. 2(a). A total of 25 circular plates (outer diameter 70 mm, 1 mm thick) are utilized to generate a homogeneous electrostatic field, which are linked with precision resistors to divide the voltages, and velocity focusing is achieved simultaneously for both electrons and ions in two opposite directions. It should be mentioned that all lenses and two TOF tubes are fixed together with four Ti alloy shores symmetrically located close to the outer edges of electrode plates, and adjusted very carefully to keep all electrodes and tubes homocentric. The two repeller electrodes of ionization region are separated by aluminum oxide spacers of 12 mm length, while the spacers between the other extractor electrodes are 6 mm. As mentioned above, a low extraction field is generally required for good electron energy resolution in TPES, while high collection efficiency for ions needs a strong extraction field. This contradiction causes a balance for us to choose a moderate extraction field, which is typically 15 V cm^{-1} as 18 V difference on 12 mm length shown in Fig. 2(a), and this extraction field will be used in the following sections unless otherwise noted. At the 15 V cm^{-1} extraction field, the electrostatic potential of ionization region is kept to be ground, and the drift tubes of electron and ion are of +18 and -514 V, respectively. In order to maintain enough response efficiency of electron detector,⁴⁰ the incoming surface of micro-channel plates (MCP) is set on a potential of +300 V. Similarly, the 1800 eV impact energy for ions is obtained after passing through a grid at the end of ion drift tube to guarantee response efficiency of ion detector.

TABLE I. Ratios of hot electrons with different kinetic energies simulated in present spectrometer with the repelling field, where the 20 V cm^{-1} and 15 V cm^{-1} extraction fields are applied, respectively. The corresponding data of previous results in Ref. 31 are involved as well. (Radiuses are obtained by simulation with SIMION 3D program.)

Ionization region/mm ³	Kinetic energy of electron/meV	Maximal radius of velocity imaging on detector/mm			Ratio of detected hot electrons of the present spectrometer ^b
		Ref. 31 ^a	Present		
			20 V cm^{-1}	15 V cm^{-1}	
$1 \times 3 \times 4$	10	2.1	4.5	5.3	6.3%
	20	2.8	6.3	7.3	4.4%
	30	3.5	7.7	8.8	3.6%
	50	...	9.8	11.3	2.8%

^aData are read from Fig. 2 in Ref. 31, where the extraction electric field is 20 V cm^{-1} .

^bData are computed at the extraction field of 15 V cm^{-1} .

The overall flight lengths for electrons and ions from ionization region to each detector are 250 and 380 mm, respectively.

Compared with previous experimental apparatus,^{3,4,16–19,36,37} four special designs have been applied to the present TPEPICO imaging spectrometer in order to obtain a high energy resolution of electrons, double velocity imaging effects for both electrons and ions, and the improvement of coincidence efficiency. First, a repelling electric field involving an extra electrode is applied to magnify the images of electrons. Generally, an accelerating field is used in VMI of electrons, so electrons will reach the detector in several ten nanoseconds. In this case, energetic electrons only expend a little bit and many of them can pass through the aperture in front of the detector and be recorded mistakenly as threshold electrons, which will generate fake structures in TPES and cause the large false coincidence in TPEPICO experiments. Here, an extra electrode is located behind the three-electrode structure of VMI to constitute a repelling electric field, which will prolong the arrival time of electrons to about 120 ns and thereby magnify the electron images. The function of this deigned extra electrode is similar to the magnifying lens described in Ref. 41. The detailed potentials of this repelling sequence are presented in Fig. 2(a). As shown in Fig. 2(b), all threshold electrons produced in the ionization region ($1 \times 3 \times 4 \text{ mm}^3$) are collected into the 1 mm diameter aperture at the end of drift tube through a sequence of accelerating then decelerating processes, while energetic electron clouds expand much more. As a result, only a few energetic electrons ($\sim 3\%$) with initial velocity vectors along the TOF axis will pass through the aperture and induce the false coincidence events. In order to clearly exhibit advantage of the repelling field, a typical accelerating field and the present repelling field have been simulated, respectively, and compared within our TOF geometry using Simion program. At the same extraction field of 15 V cm^{-1} , electrons with 50 meV initial kinetic energy perpendicular to the TOF axis are focused to a ring of radius 7.8 mm on the detector with the accelerating field, while they are projected into a radius 11.3 mm ring with the present repelling field. Obviously, the ratio of the energetic electrons passing through the aperture can be reduced significantly when using the repelling field. Furthermore, to compare with the previous study,³¹ ring radiuses of the focusing images of energetic

electrons with 10, 20, 30, and 50 meV kinetic energies are summarized in Table I. The ratios of energetic electrons passing through the aperture from our simulations are listed as well. In Table I, ring radiuses of images in Baer's results are read approximately from Fig. 2 in Ref. 31, where the extraction field of TOF is of 20 V cm^{-1} . As indicated in Table I, the energetic electron cloud in present spectrometer expands much bigger than that in Ref. 31.

Second, VMI has been employed on both electrons and ions. When photon energy exceeds dissociation limits of ion, DPI process of molecule will probably happen. Among previous TPEPICO experiments,^{3,4,16–19,36,37} a linear TOF mass spectrometer has been combined to detect ions. The KERD of fragment ion can be derived from simulation of the spread shape of corresponding TOF mass peak.^{4,19,38,39} However the KERD obtained from the method is characterized by an energy resolution which varies inversely with the release energy, and thus it is very difficult to get precise internal energy distribution of fragments.¹³ In the present TPEPICO spectrometer, we have applied VMI technique on both electrons and ions. VMI of electrons can improve the collection efficiency and energy resolution of threshold electrons, while VMI of ions has an ability of probing the full three-dimensional (3D) velocity distribution of ions, in contrast to the conventional TOF method. Moreover, since VMI has a better energy resolution and angular distribution, more information like internal energy distribution and vector correlations can be revealed as well.

Third, all electrodes are totally open without any grids. Generally, grids are used in TOF mass spectrometer to achieve a high mass resolution, and even in the most recent imaging TPEPICO spectrometers grids are still used in the TOF of ion portion.^{36,37} In the recent experiments,^{36,37} VMI is only applied to analyze photoelectrons, and the energy resolution of TPES after subtracting contribution from energetic electrons is improved. However, when the spectrometers are utilized for TPEPICO experiments, ions will be scattered by grids on the flight ways and thus the coincidence efficiency will be reduced. The more serious demerit of using grids in imaging experiment is that grids will distort the ion trajectories, and hence the kinetic energy resolution of ion will be decreased significantly. In order to discard grids in the present spectrometer, a precise simulation has been performed with all open electrodes to obtain VMI for both elec-

trons and ions simultaneously. As shown in Fig. 2(c), all ions with the same initial momentum produced at different positions of ionization region are focused onto the same point of surface of ion detector. The simulated kinetic energy resolution of ions is about 2.5% of $\Delta E/E$.

Moreover, a set of stainless rings connected with the corresponding plates are used to block the surrounding electric field. The similar design has been employed in previous slow electron imaging, where these rings have been proved to improve the quality of the electric fields between the electrodes.⁴² As our simulation shows, the ion cloud expands much when flying toward detector at moderate extraction field, especially for the ions with high kinetic energy. Their trajectories are somewhat close to the inner edges of electrodes, as shown in Fig. 2(c). If the four Ti alloy shores have a large potential difference from the electrodes, the potential contour will change dramatically in the nearby region of inner edge of electrodes, and hence the observed ion imaging will be distorted. In order to avoid this distortion, a set of stainless rings connected with the corresponding plates are used to shield the outer potential, as shown in Fig. 2(a).

D. Single-start/multiple-stop data acquisition mode

Photoionization events are recorded in our experiments with a special counting mode named “single-start/multiple-stop (SM) data acquisition,”⁴³ in which the electrons passing the central aperture at the end of electron drift tube provide start signals for measuring TOFs of ions, and a counter (FAST Comtec, Germany, P7888) records relative time of every “stop” ion signals. An important benefit of the P7888 counter is that it automatically neglects any new start signals and records all ion stop signals during the selected time range. Thus, signals of true coincident ions are augmented at a certain range of flight time, while the false coincident ions distributed randomly. The random distribution of false coincident ions seems opposite to the conclusion of Bodi *et al.*⁴³ that the false coincidence background is not uniform in the SM spectra. However, as shown in mass spectrum of Xe⁺ (Fig. 4), the false coincidence ions are observed to distribute randomly (uniform) even though the collection efficiencies are relatively high. The seeming disagreement between our observations and Bodi *et al.*'s simulation should originate from the ionization frequencies, since false coincidence background depends on ionization frequency and collection efficiencies.⁴³ In our experiments, the photon flux is manually decreased to maintain an average ionization event frequency of less than 1 kHz, and thus the time interval between two ionization events is more than 1000 μ s, while in Bodi *et al.*'s simulation, the ionization event frequency was assumed to be 1000 kHz. Since in our experiments the flight times of electrons and ions are about 120 ns and 20 μ s (e.g., 15 μ s for Ar⁺, \sim 23 μ s for Xe⁺), respectively, we can ensure that the measured mass spectrum mostly comes from single ionization event, in other words, almost only one ionization event happens in each data acquisition cycle.

The ions are focused through VMI onto the surface of MCPs (Burle Industries, 40 mm diameter) and further mapped by Phosphor Screen (Burle Industries, P20). The TE-

cooling charge coupled device (CCD) detector (Andor, DU934N-BV) is used to record the images, which reflect the velocity radial and angular distribution of ions. For TPEPICO imaging experiment, a pulsed high voltage of 1800 V is applied to the front surface of MCP detector as a mass gate in Fig. 2(a), whose duration can be varied from 50 ns to dc depending on the arrival time of ions.

III. EXPERIMENTAL RESULTS AND DISCUSSION

A. Threshold photoelectron spectra of xenon and argon

There are many high- n Rydberg states above the IEs of xenon and argon, which converge to the $^2P_{1/2}$ state of cations.^{21,22,31} These Rydberg states will undergo autoionization to the $^2P_{3/2}$ ground ionic state and produce energetic electrons. As mentioned above, the true threshold photoelectrons are often contaminated by energetic electrons, so that suppressing the contamination is an important factor of a threshold photoelectron spectrometer. Here, Xe and Ar atoms are used as benchmarks to test the present apparatus, and their TPES are recorded to get the energy resolution of threshold electron.

In Fig. 3, the TPES of Xe in 12.05–13.52 eV photon energy range and Ar in 15.72–16.00 eV are presented, where the spectral scan step is 2 meV. For comparison, the photoionization efficiency (PIE) curves of Xe and Ar are shown as well in Fig. 3. It should be noted that these TPES are obtained directly without any subtraction. As shown in Fig. 3(a), there are few electron counts (almost equal to zero) between the $^2P_{3/2}$ and $^2P_{1/2}$ peaks in the TPES of Xe, indicating that almost all energetic electrons have been dispersed and blocked by the 1 mm diameter aperture in front of the electron detector.

In order to show the suppressing effect for energetic electrons with low kinetic energies in present spectrometer, the 12s' Rydberg state of Ar (15.798 eV, just 38 meV above IE)^{21,22} is chosen to estimate the suppression ratio. As shown in Fig. 3(b), the 15.763 and 15.798 eV peaks are of nearly equal intensity in the PIE curve, while their relative intensities in the TPES change significantly with a ratio of 1:0.06. Furthermore, the hot electrons with energies of around 50 meV are suppressed to about 2%, as indicated in Fig. 3(b), which is consistent with the simulation in Table I. Therefore, the suppression of energetic electrons in present spectrometer is acceptable.

The TPES energy resolution with present apparatus is obtained from Fig. 3(b). The 11s' Rydberg state of Ar atom locates just 3 meV above the $^2P_{3/2}$ ionic state, and its autoionization produces 3 meV hot electron. Unfortunately, this hot electron cannot be discriminated in present TPES due to the energy resolution. We use the width of the $^2P_{1/2}$ ionic state to illustrate our TPES energy resolution, since the profile of $^2P_{3/2}$ state is potentially modulated by the nearby Rydberg states.⁴ The measured energy resolution is 9 meV from Fig. 3(b) which is larger than the resolution of light source (6 meV), indicating that the instrument function is also an important factor for the electron energy resolution in present experiments.

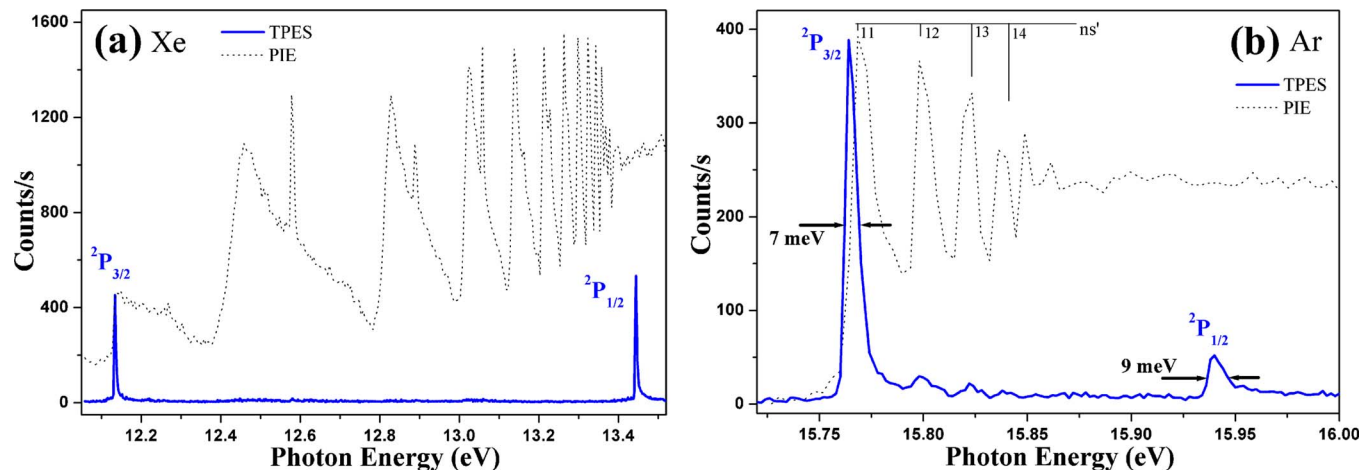


FIG. 3. (Color online) TPES (in blue solid) and PIE (in black dot) curves of xenon and argon. (a) TPES and PIE curve of Xe in 12.05–13.52 eV range; (b) TPES and PIE curve of Ar in 15.72–16.00 eV range.

B. Mass spectrum of xenon in TPEPICO experiment

Mass resolving power is one of the most important parameters of a mass spectrometer. We measured the resolving power with the mass spectrum of xenon isotopes. When fixing the photon energy at the IE position of Xe, 12.130 eV, we recorded the TPEPICO mass spectrum of Xe^+ , as shown in Fig. 4. All of nine isotopes of Xe are clearly observed with intensities of their nature abundance, and the S/N ratio for $^{132}\text{Xe}^+$ is about 200. The mass resolving power of $M/\Delta M$ is measured to be above 900, which is high enough to match our designs. As we know, in velocity imaging experiments (especially the time-sliced imaging), the fragment ion clouds generally spread along the TOF axis. Therefore, the mass resolving power for ions with kinetic energies will decrease. We have calculated the change of mass resolution for the fragmentation of ethanol ion ($\text{C}_2\text{H}_5\text{OH}^+$) using the Simion program. Even for fragment ion $\text{C}_2\text{H}_5\text{O}^+$ with total released kinetic energy of 1.8 eV, the result still shows a satisfied mass resolution to distinguish M-1 fragment in the TOF mass spectrum. It means that this spectrometer operated under velocity imaging conditions still has a sufficient mass resolving power.

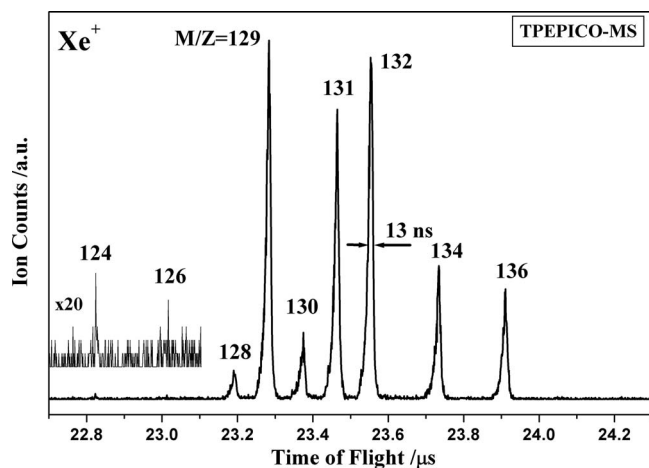


FIG. 4. TOF spectrum of xenon isotopes measured in coincidence with threshold electrons at the IE position of 12.130 eV.

When recording the intensity of a mass-selected ion and scanning the VUV photon energy, a mass-selected TPEPICO spectrum can be acquired. This spectrum should be the same as TPES, if gas sample is pure and does not dissociate. For instance, both structures of the TPES and TPEPICO spectrum of Ar in 15.75–16.10 eV energy range are almost identical, from which the coincidence rate can be obtained and collection efficiency of ions can be derived. In our experiment, the counting rate E of threshold photoelectrons of Ar at 15.760 eV is 313 counts/s, and the coincidence rate C in TPEPICO spectrum is 194 counts/s, thus the collection efficiency of Ar^+ is determined to be 62% from C/E .¹³

If there are more than one ion species, the mass-selected TPEPICO spectrum will be very useful to identify contributors of each resonance bands in TPES. Therefore, this working mode is very suitable and powerful for investigating DPI dynamics of molecules and/or analyzing of a mixture sample. We have performed a series of benchmark experiments for mixture samples, such as Ar/Xe/Ne (1:1:18) mixture gas. For instance, all resonance bands corresponding to Ar and Xe have been observed in the TPES of the Ar/Xe/Ne mixture gas. When the photon energy is above the IEs of Xe and Ar, both Xe^+ and Ar^+ exist simultaneously. If the mass gates are chosen for detecting Xe^+ or Ar^+ , the mass-selected TPEPICO spectra are recorded individually and consistent with the TPES of pure Xe or Ar gases, respectively. The details of these experiments will be analyzed and discussed in a future article.

C. Imaging of argon ions in TPEPICO experiment

As a VMI apparatus with the perpendicular geometry of TOF axis to MB, the focusing power of ions needs to be checked. As described above, when the selected ions reach the detector, a pulsed high voltage is applied on MCPs as a mass gate, and the ion velocity images are recorded by the CCD camera.

Photoionization of Ar is chosen as a benchmark to evaluate the velocity focusing power and estimate the translational temperature of MB. The TPEPICO image of Ar^+ is recorded at the IE position of Ar (15.760 eV), and presented in Fig. 5.

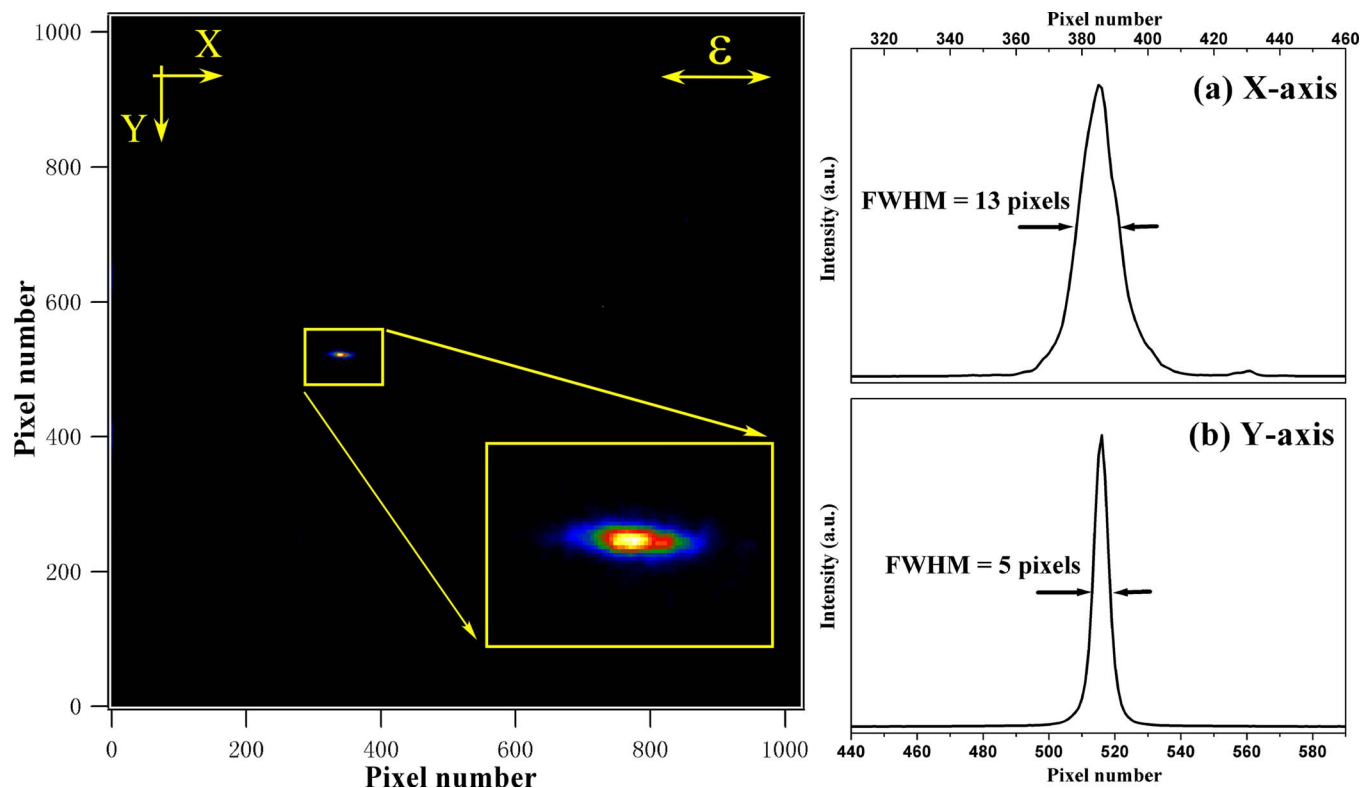


FIG. 5. (Color online) TPEPICO velocity imaging of Ar at the IE position of 15.760 eV with extraction field of 15 V cm⁻¹. Stagnation pressure of Ar/Ne mixture (1:20) is 1.2×10^5 Pa. (a) Intensity distribution along the direction of MB (*x*-axis); (b) Intensity distribution along the *y*-axis direction.

The MB flows along the *x*-axis from right to left, and the VUV light propagates along the *y*-axis. For this configuration, the FWHMs along the *x*-axis and *y*-axis of image in Fig. 5 reflect the velocity focusing power. It can be clearly seen that the recorded image is not at the center of CCD. The displacement corresponds to flow downstream distance of ions with a certain speed along *x*-axis. With this position offset and the Ar⁺ flight time, the center-of-mass (CM) velocity of MB is calculated to be about 766 m s⁻¹. Due to velocity distribution along the direction of MB, the spatial resolution in the *x*-axis direction is limited in some extent.^{33,44} In Fig. 5(a), the ion image along the *x*-axis shows a FWHM of 13 pixels, which corresponds to 0.507 mm width on the MCP surface. A Gaussian fit with the Boltzmann velocity distribution^{44,45} indicates that the MB parallel translational temperature is about 10 K, which is close to that of a typical supersonic beam. In other words, this FWHM along the direction of MB is difficult to be eliminated in a TOF mass spectrometer with perpendicular geometry.^{33,44}

As shown in Fig. 5(b), the width of ion image along the *y*-axis is much narrower than that along the direction of MB. The FWHM of image perpendicular to MB is only five pixels, which corresponds to 0.195 mm width on the MCP surface. Indeed, it is very close to the size that expected in the Simion simulation, 0.16 mm on detector surface. Thus, the narrow velocity distribution perpendicular to the direction of MB means a satisfied focusing power of VMI and very limited expansion of MB downstream the nozzle due to the skimmer.

In principle, reducing the size of photoionization region can improve the spatial resolution of ion imaging. However,

in present spectrometer, the photoionization region is of about $1 \times 3 \times 4$ mm³ as mentioned above and difficult to be further reduced. Although the region is much bigger than that in pulsed laser photoionization experiments, the spatial resolution of present velocity imaging still seems to be satisfied.

D. TPEPICO imaging investigation on DPI of O₂

A major aim of present spectrometer is to investigate DPI dynamics of molecules, especially for the higher energy states above dissociation limits of ions. In this case, usually more than one product channels are open and the mass-selected TPEPICO spectroscopy is suitable to detect every fragment ions as described above. In order to obtain whole information of DPI dynamics, the branch ratios, kinetic, and internal energy distributions of fragment ions are necessary to measure exactly. Thus, the VMI of ions seems to be the most suitable tool for our aim as it can provide better momentum resolution and angular distribution. As a benchmark, we have accomplished a mass-selected TPEPICO imaging experiment to investigate the DPI of oxygen molecule.

A continuous MB of the O₂/Ne (1:20) mixture gas is generated by supersonic jet with a backing pressure of 1.5×10^5 Pa. The measured TPES of O₂ molecule is presented in Fig. 6, where two vibronic progresses are identified and correspond respectively to vibrational excitations of the $b^4\Sigma_g^-$ and $B^2\Sigma_g^-$ states of O₂⁺. These two resonance progresses have been studied extensively and assigned definitely before.^{46–50} The lower vibronic states ($v=0–3$) of the $b^4\Sigma_g^-$ state of O₂⁺ are bounding, while the $B^2\Sigma_g^-$ ($v=0–3$) states are fully predissociative to produce fragments of

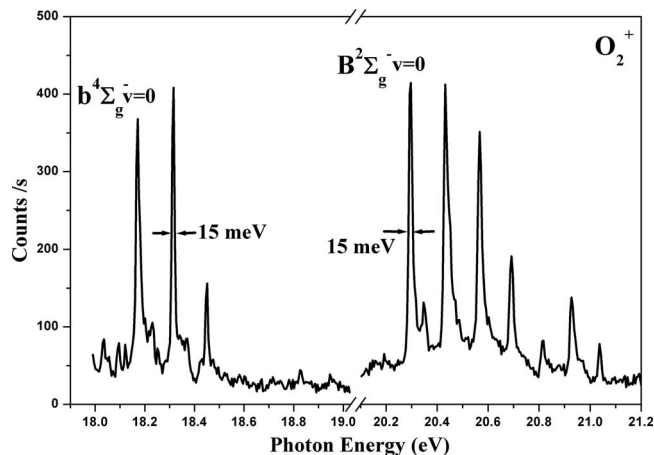


FIG. 6. TPEPICO of O_2 molecule in 18.0–21.2 eV energy range measured with extraction field of 15 V cm^{-1} .

$O^+(^4S_0)$ and $O(^3P)$, as the dissociation limit of $O^+(^4S_0)$ and $O(^3P)$ is of 18.733 eV from the neutral O_2 molecule.^{48,49}

To measure the O^+ image from DPI process of O_2 , the basic working mode is the same as that in imaging of Ar^+ described in Sec. III C. The VUV photon energy is fixed at 20.298 eV, which is corresponding to resonance wavelength of the $B^2\Sigma_g^-(v=0)$ state of O_2^+ , and the TPEPICO image of O^+ with KER of 0.783 eV is recorded subsequently and exhibited in Fig. 7.^{48–50} The MB flows along the x -axis, and the polarization of photons is along this direction as well. With the CM speed of MB along x -axis, the center of image locates at the downstream somewhere related with the ion TOF. At the extraction field of 15 V cm^{-1} , the flight time of O^+ fragment packet with the 0.783 eV kinetic energy spreads about 800 ns, so that a wide mass gate of over 800 ns is

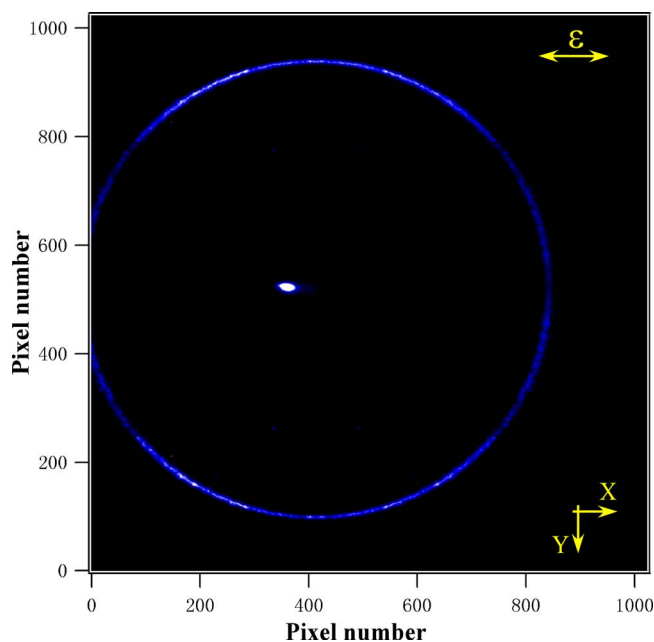


FIG. 7. (Color online) Time-sliced image of O^+ measured in TPEPICO mode at 20.298 eV with extraction field of 15 V cm^{-1} , where a 60 ns mass gate is used. The center bright spot corresponds to the false coincidence image of parent O_2^+ , and the outer ring reflects the velocity spatial and angular distributions of O^+ from the dissociation $O_2^+(B^2\Sigma_g^-) \rightarrow O^+(^4S_0) + O(^3P)$.

needed to collect all ions for constructing a two-dimensional (2D) image. The 3D ion velocity distribution can be acquired from inverse Abel transformation of the 2D raw image.^{33–35} However, when a mass gate is utilized to select ions, the wider the mass gate is, the more false coincidence events are involved. In present experiments, the false coincidence events coming from energetic electrons are not fully suppressed and construct a nonzero background in the TPEPICO mass spectrum, which is mainly contributed from parent O_2^+ without kinetic energy. Therefore, it is difficult to get a 3D velocity distribution of O^+ from inverse Abel transformation of the image. In order to overcome this problem, the time-sliced imaging technique^{51–56} is applied to acquire the 3D velocity distribution of ions directly. Because of no inverse Abel transformation needed, the higher kinetic energy resolution and the better S/N ratio are expected.^{51–56} A typical sliced O^+ image in Fig. 7 is recorded with a mass gate of 60 ns, where the image has been accumulated for almost 4 h in experiments. In the y -axis direction, velocity resolving power $\Delta V/V$ of O^+ fragment is 1.2% as the FWHM of five pixels divided by radius of 419 pixels, and the corresponding kinetic energy resolving power $\Delta E/E$ is of double $\Delta V/V$ and better than 3%, which is slightly above the simulated result (2.5%) and close to that of sliced imaging with pulsed lasers.^{55,56}

An outer ring with diameter of 838 pixels and a bright spot close to center are observed in Fig. 7, and both are slightly excentric. In the photoexcitation of an oxygen molecule at 20.298 eV, there are two possible ionization pathways, one is to produce an energetic electron and O_2^+ of almost zero kinetic energy, and the other is undergoing a DPI process to produce $O^+(^4S_0)$ and $O(^3P)$ fragments with a threshold electron. Thus, the O^+ as the major spectral carrier of the mass-selected TPEPICO spectrum contributes to the outer ring, while the O_2^+ from the first ionization pathway composes the false coincidence signals in experiment and contributes the bright spot. It means that the different carrier ions for the bright spot and the outer ring lead to the excentric image in Fig. 7. The bright spot from the O_2^+ seems very similar to the TPEPICO image of Ar^+ in Fig. 5. Although both O^+ and O_2^+ ions have the same CM velocity, the arrival times of O^+ and O_2^+ are absolutely different. The O_2^+ needs more time to reach the detector, so that its image center is far downstream from the center of CCD, compared with that of O^+ . Through distances of the bright spot and the center of outer ring from the center of CCD, the CM speed can be calculated to be about 960 m s^{-1} using the TOFs of O^+ ($8.194 \mu\text{s}$) and O_2^+ ($11.587 \mu\text{s}$).

IV. CONCLUSIONS

Here, we present a novel TPEPICO imaging spectrometer at the U14-A beamline of the Hefei National Synchrotron Radiation Laboratory. In this spectrometer, VMI has been designed for both electrons and ions, in which a repelling electric field using an extra lens is used for magnifying electron images instead of traditional accelerating optics. As a result, contribution of the false coincidence from energetic

electrons has been suppressed efficiently, and thus the energy resolution of TPES has been increased significantly.

As indicated by experiments with Ar, Xe, and O₂ molecules, the present apparatus has been confirmed to work steadily and properly. This apparatus has three specific functions for future studies on the photoionization and DPI of gas molecules and clusters:

- (a) TPES of molecules can be measured conveniently. Since the energetic electrons are dispersed by the repelling field and blocked by the aperture before detector, almost only threshold electrons are detected. As simulated with Simion program and tested by Ar and Xe experiments, only 2% “hot” electrons (with kinetic energy of over 50 meV) exists in TPES with a moderate extraction field of 15 V cm⁻¹. The typical energy resolution of TPES is measured to be 9 meV. Through the TPES experiments, the IEs of molecules can be directly determined, and more information like molecular structures and vibrational frequencies of cations can be obtained subsequently, which seems much more convenient and effective than that of using pulsed lasers.^{57–59}
- (b) TPEPICO spectroscopy of molecules can be recorded. Threshold electrons are used as the start signals for measuring the TOFs of ions, and the TPEPICO mass spectra are measured consequently. The observed mass resolving power for the spectrometer is above 900 of $M/\Delta M$ as indicated by the experiments of Xe isotopes. If the precursors are gas mixtures, the mass-selected TPEPICO spectra can be recorded with scanning photon energy and contribution of each component can be picked up. This function will also be very useful for investigation of clusters because they are usually generated with a lot of mass species in MB.
- (c) DPI dynamics of molecules can be investigated. When the apparatus works in coincidence mode and the photon energy is fixed at an appointed resonance wavelength of molecule ion, the TPEPICO mass spectrum can be measured, and then VMI of the mass-selected fragment ion can be recorded consequently. The velocity distributions of fragment ions in DPI processes will be derived accurately from the images. In this mode, dissociation dynamics of the state-selected ions can be studied in detail, and the bonding energy of ions will be obtained. The benchmark experiment of oxygen molecule at 20.298 eV indicates the kinetic energy resolution of the present TPEPICO imaging spectrometer is better than 3% of $\Delta E/E$.

ACKNOWLEDGMENTS

The authors would like to thank Dr. C. Y. Ng for his kind suggestions of experiments. This research was supported by the National Natural Science Foundation of China (Grant Nos. 20533070 and 20603033) and the National Key Basic Research Special Foundation (NKBRF) (Grant No.2007CB815204). Authors would like to specially acknowledge the financial support from the Instrument Devel-

oping Project of the Chinese Academy of Sciences (Grant No. YZ200763) and the CAS Project of the Knowledge Innovation Program (Grant No. KJCX2-YW-N07) as well.

- ¹ *Vacuum Ultraviolet Photoionization and Photodissociation of Molecules and Clusters*, edited by C. Y. Ng (World Scientific, Singapore, 1991).
- ² C. Y. Ng, in *Photoionization and Photodetachment*, Advanced Series in Physical Chemistry Vol. 10, edited by C. Y. Ng (World Scientific, Singapore, 1999).
- ³ C. Y. Ng, *Annu. Rev. Phys. Chem.* **53**, 101 (2002).
- ⁴ K. M. Weitzel and J. Mähner, *Int. J. Mass Spectrom.* **214**, 175 (2002).
- ⁵ T. A. Cool, A. McIlroy, F. Qi, P. R. Westmoreland, L. Poisson, D. S. Peterka, and M. Ahmed, *Rev. Sci. Instrum.* **76**, 094102 (2005).
- ⁶ J. N. Shu, K. R. Wilson, M. Ahmed, and S. R. Leone, *Rev. Sci. Instrum.* **77**, 043106 (2006).
- ⁷ S. S. Wang, R. H. Kong, X. B. Shan, Y. W. Zhang, L. S. Sheng, Z. Y. Wang, L. Q. Hao, and S. K. Zhou, *J. Synchrotron Radiat.* **13**, 415 (2006).
- ⁸ C. Q. Huang, B. Yang, R. Yang, J. Wang, L. X. Wei, X. B. Shan, L. S. Sheng, Y. W. Zhang, and F. Qi, *Rev. Sci. Instrum.* **76**, 126108 (2005).
- ⁹ B. Brehm and E. V. Puttkamer, *Z. Naturforsch.* **22A**, 8 (1967).
- ¹⁰ J. H. D. Eland, *Int. J. Mass Spectrom. Ion Phys.* **12**, 389 (1973).
- ¹¹ A. S. Werner and T. Baer, *J. Chem. Phys.* **62**, 2900 (1975).
- ¹² R. Stockbauer, *J. Chem. Phys.* **58**, 3800 (1973).
- ¹³ T. Baer, in *Gas Phase Ion Chemistry*, edited by M. T. Bowers (Academic, New York, 1979), Vol. 1.
- ¹⁴ R. Thissen, C. Alcaraz, J. Hepburn, M. Vervloet, and O. Dutuit, *Int. J. Mass Spectrom.* **199**, 201 (2000).
- ¹⁵ Q. Zha, R. N. Hayes, T. Nishimura, G. G. Meisels, and M. L. Gross, *J. Phys. Chem.* **94**, 1286 (1990).
- ¹⁶ M. Richard-Viard, O. Atabek, O. Dutuit, and P. M. Guyon, *J. Chem. Phys.* **93**, 8881 (1990).
- ¹⁷ G. K. Jarvis, K. M. Weitzel, M. Malow, T. Baer, Y. Song, and C. Y. Ng, *Rev. Sci. Instrum.* **70**, 3892 (1999).
- ¹⁸ B. Sztáray and T. Baer, *Rev. Sci. Instrum.* **74**, 3763 (2003).
- ¹⁹ D. P. Seccombe, R. Y. L. Chim, G. K. Jarvis, and R. P. Tuckett, *Phys. Chem. Chem. Phys.* **2**, 769 (2000).
- ²⁰ T. Baer, W. B. Peatman, and E. W. Schlag, *Chem. Phys. Lett.* **4**, 243 (1969).
- ²¹ R. Spohr, P. M. Guyon, W. A. Chupka, and J. Berkowitz, *Rev. Sci. Instrum.* **42**, 1872 (1971).
- ²² R. I. Hall, A. McConkey, K. Ellis, G. Dawber, L. Avaldi, M. A. Macdonald, and G. C. King, *Meas. Sci. Technol.* **3**, 316 (1992).
- ²³ P. A. Hatherly, M. Stankiewicz, K. Codling, J. C. Creasey, H. M. Jones, and R. P. Tuckett, *Meas. Sci. Technol.* **3**, 891 (1992).
- ²⁴ D. M. Smith, R. P. Tuckett, K. R. Yoxall, K. Codling, P. A. Hatherly, J. F. M. Aarts, and M. Stankiewicz, *J. Chem. Phys.* **101**, 10559 (1994).
- ²⁵ T. Baer, P. M. Guyon, I. Nenner, A. Tabché-Fouhaillé, R. Botter, L. F. A. Ferreira, and T. R. Govers, *J. Chem. Phys.* **70**, 1585 (1979).
- ²⁶ F. Merkt, P. M. Guyon, and J. W. Hepburn, *Chem. Phys.* **173**, 479 (1993).
- ²⁷ F. Merkt and P. M. Guyon, *J. Chem. Phys.* **99**, 3400 (1993).
- ²⁸ K. M. Weitzel and F. Guthe, *Chem. Phys. Lett.* **251**, 295 (1996).
- ²⁹ G. K. Jarvis, R. C. Shiell, J. W. Hepburn, Y. Song, and C. Y. Ng, *Rev. Sci. Instrum.* **71**, 1325 (2000).
- ³⁰ X. M. Qian, K. C. Lau, G. Z. He, C. Y. Ng, and M. Hochlaf, *J. Chem. Phys.* **120**, 8476 (2004).
- ³¹ T. Baer and Y. Li, *Int. J. Mass Spectrom.* **219**, 381 (2002).
- ³² T. Baer, B. Sztáray, J. P. Kercher, A. F. Lago, A. Bödi, C. Skull and D. Palathinkal, *Phys. Chem. Chem. Phys.* **7**, 1507 (2005).
- ³³ A. T. J. B. Eppink and D. H. Parker, *Rev. Sci. Instrum.* **68**, 3477 (1997).
- ³⁴ D. W. Chandler and D. H. Parker, *Adv. Photochem.* **25**, 59 (1999).
- ³⁵ J. A. Davies, J. E. LeClaire, R. E. Continetti, and C. C. Hayden, *J. Chem. Phys.* **111**, 1 (1999).
- ³⁶ G. A. Garcia, H. Soldi-Lose, and L. Nahon, *Rev. Sci. Instrum.* **80**, 023102 (2009).
- ³⁷ A. Bödi, M. Johnson, T. Gerber, Z. Gengeliczki, B. Sztáray, and T. Baer, *Rev. Sci. Instrum.* **80**, 034101 (2009).
- ³⁸ R. Vasudev, R. N. Zare, and R. N. Dixon, *J. Chem. Phys.* **80**, 4863 (1984).
- ³⁹ H. Xu, Y. Guo, Q. Li, Y. Shi, S. Liu, and X. Ma, *J. Chem. Phys.* **121**, 3069 (2004).
- ⁴⁰ J. L. Wiza, *Nucl. Instrum. Methods* **162**, 587 (1979).
- ⁴¹ H. L. Offerhaus, C. Nicole, F. Lépine, C. Bordas, F. Rosca-Pruna, and M. J. J. Vrakking, *Rev. Sci. Instrum.* **72**, 3245 (2001).
- ⁴² A. Osterwalder, M. J. Nee, J. Zhou, and D. M. Neumark, *J. Chem. Phys.*

- 121**, 6317 (2004).
- ⁴³ A. Bödi, B. Sztáray, T. Baer, M. Johnson, and T. Gerber, *Rev. Sci. Instrum.* **78**, 084102 (2007).
- ⁴⁴ D. Irimia, R. Kortekaas, and M. H. M. Janssen, *Phys. Chem. Chem. Phys.* **11**, 3958 (2009).
- ⁴⁵ *Molecular Beams*, edited by N. F. Ramsey (Oxford University Press, New York, 1985).
- ⁴⁶ D. H. Parker and A. T. J. B. Eppink, *J. Chem. Phys.* **107**, 2357 (1997).
- ⁴⁷ B. Buijsse, W. J. van der Zande, A. T. J. B. Eppink, D. H. Parker, B. R. Lewis, and S. T. Gibson, *J. Chem. Phys.* **108**, 7229 (1998).
- ⁴⁸ T. Akahori, Y. Morioka, M. Watanabe, T. Hayaishi, K. Ito, and M. Nakamura, *J. Phys. B* **18**, 2219 (1985).
- ⁴⁹ M. Richard-Viard, O. Dutuit, M. Lavollée, T. Govers, P. M. Guyon, and J. Durup, *J. Chem. Phys.* **82**, 4054 (1985).
- ⁵⁰ M. Evans, S. Stimson, C. Y. Ng, C.-W. Hsu, and G. K. Jarvis, *J. Chem. Phys.* **110**, 315 (1999).
- ⁵¹ K. Tonokura and T. Suzuki, *Chem. Phys. Lett.* **224**, 1 (1994).
- ⁵² C. R. Gebhardt, T. P. Rakitzis, P. C. Samartzis, V. Ladopoulos, and T. N. Kitsopoulos, *Rev. Sci. Instrum.* **72**, 3848 (2001).
- ⁵³ L. Dinu, A. T. J. B. Eppink, F. Rosca-Pruna, H. L. Offerhaus, W. J. van der Zande, and M. J. J. Vrakking, *Rev. Sci. Instrum.* **73**, 4206 (2002).
- ⁵⁴ V. Dribinski, A. Ossadtchi, V. A. Mandelshtam, and H. Reisler, *Rev. Sci. Instrum.* **73**, 2634 (2002).
- ⁵⁵ D. Townsend, M. P. Minitti, and A. G. Suits, *Rev. Sci. Instrum.* **74**, 2530 (2003).
- ⁵⁶ J. J. Lin, J. Zhou, W. Shiu, and K. Liu, *Rev. Sci. Instrum.* **74**, 2495 (2003).
- ⁵⁷ H. Xu, Y. Guo, Q. Li, S. Liu, X. Ma, J. Liang, and H. Li, *J. Chem. Phys.* **119**, 11609 (2003).
- ⁵⁸ L. Zhang, Z. Wang, J. Li, F. Wang, S. Liu, S. Yu, and X. Ma, *J. Chem. Phys.* **118**, 9185 (2003).
- ⁵⁹ L. Zhang, F. Wang, Z. Wang, S. Yu, S. Liu, and X. Ma, *J. Phys. Chem. A* **108**, 1342 (2004).